catalysts

MDPI

Article

Steric Effects of Mesoporous Silica Supported Bimetallic Au-Pt Catalysts on the Selective Aerobic Oxidation of Aromatic Alcohols

Jun Yan [1], Longlong Shan [1,*], Xiaoli Gu [1,*], Xingguang Zhang [1,2,*] and Junmeng Cai [3]

[1] College of Chemical Engineering, Nanjing Forestry University, No. 159 Longpan Road, Nanjing 210037, China; junyan@njfu.edu.cn
[2] Department of Chemistry, School of Science, University of Shanghai for Science and Technology, 516 Jungong Road, Shanghai 200093, China
[3] Biomass Energy Engineering Research Center, School of Agriculture and Biology, Shanghai Jiao Tong University, 800 Dongchuan Road, Shanghai 200240, China; jmcai@sjtu.edu.cn
* Correspondence: shanlonglong@njfu.edu.cn (L.S.); guxiaoli@njfu.edu.cn (X.G.); x.g.zhang@usst.edu.cn (X.Z.)

Received: 21 September 2020; Accepted: 9 October 2020; Published: 15 October 2020

Abstract: Three series of catalysts consisting of gold (Au), platinum (Pt), or gold-platinum bimetallic nanoparticles (NPs) with controlled sizes (Au NPs 10 ± 2 nm, Pt NPs 6 ± 2 nm) anchored on hierarchical micro-/meso-/macroporous silica were successfully developed and systematically evaluated for the selective oxidation of aromatic alcohols to their corresponding aldehydes. The catalysts were prepared by the sol-immobilization method using as-made Au NPs and/or Pt NPs colloids; the silica supports were prepared with controlled pore structures and the hierarchical porous structures of catalysts were created by controllable desilication via the alkaline solution of the metal colloids. The catalysts were characterized by X-ray diffraction (XRD), Brunauer-Emmett-Teller (BET), Scanning Electron Microscopy (SEM), Transmission Electron Microscopy (TEM), X-ray Photoelectron Spectroscopy (XPS), and Inductively Coupled Plasma-Mass Spectrometry (ICP-MS), and these results showed no synergistic effect between Au and Pt on boosting the catalytic performance, whereas they demonstrated a clear dependence of catalytic conversions and reaction rates on the structural porosity of Au-Pt bimetallic catalysts. Our findings could potentially inspire peer researchers and scientists to develop designer porous catalysts and processes in the selective organic conversions.

Keywords: steric effect; Au-Pt catalysts; alcohol oxidation; hierarchical porous silica

1. Introduction

Selective oxidation catalysis plays a significant role in the current chemical society for the production of key intermediates (e.g., alcohols, aldehydes, organic acids, esters, epoxides, and ketones) and valorization of biomass or bio-derived platform chemicals [1,2], contributing to green and sustainable chemistry [3]. Selective oxidation of aromatic alcohols to aldehydes is a significant process for both laboratory and commercial fine chemical production, because the aldehydes are important organic intermediates or valuable components in the industry of perfumery, dyes, pharmaceuticals, and agrochemicals [4,5]. Among these aldehydes, benzaldehyde is the most widely investigated, which is conventionally produced by hydrolysis of benzyl chloride or by vapor-phase partial oxidation of toluene, whereas these processes yield traces of chlorine impurities and a substantial quantity of waste or result in sintering of catalysts, owing to high reaction temperatures (350 °C–450 °C) [6–8]. Some chlorine-free catalytic processes have been developed, but a large amount of waste has to be disposed of due to use of more than stoichiometric quantities of strong acid or bases, inorganic

oxidants or complexes, such as dichromate, hypochlorite, permanganate, chromium(VI) oxide, and manganese(IV) oxide [9,10].

Compared with the vapor phase and homogeneous catalytic processes, liquid-phase and heterogeneous processes under mild conditions are favorable. In the metallic catalyst development for the selective oxidation of aromatic alcohols, intensive work has been focused on manipulating size effects of metal NPs [11,12], compositions [13,14], metal-support interfaces/interactions [15,16], electronic structures [17,18], or the combinational effects of these aforementioned factors [19]. These factors affect the interaction between reactants and catalysts, reaction pathways and mechanism [20–22]. In the aforementioned studies, including bimetallic or alloy-based catalysts, researchers primarily concentrate on electronic effects of catalysts or synergistic effects between multi-metal active sites on boosting the catalytic conversions; nevertheless, less attention has been paid to the steric effect of bimetallic NPs and the change in the pore structures resulted from loading of various metallic NPs.

In this study, we systematically investigated the Au-Pt/silica catalysts compared to Au/silica and Pt/silica that were prepared by a sol-immobilization method for the selective oxidation of aromatic alcohols to aldehydes. Instead of a synergistic effect between Au NPs and Pt NPs over bimetallic Au-Pt/silica catalysts, the steric effect of these nanoparticles on the catalytic performance dominated. To further confirm this phenomenon, silica supports with three different pore diameters were prepared by altering the synthetic temperatures and the silica without pores was also prepared. Through the controlled desilication effect of the alkaline solution of metal colloids, hierarchical porosity within the silica supports was created, and this desilication strategy is also popularly employed to prepare hierarchical porous materials such as zeolites [23–25]. The experimental results demonstrated that silica with larger pores showed higher catalytic performance in terms of catalytic conversion and reaction rates; moreover, the steric effect of co-existence of Au NPs and Pt NPs within silica was also confirmed. All these catalysts showed excellent selectivity toward benzaldehyde. These findings are helpful for catalyst design as the silica supports, particularly with ordered porous structures (e.g., zeolites, MOFs, MCM-41 and SBA-15) are popular for enhancing stability of metal NPs within their channel structures and simultaneously offer high surface areas and inhibit agglomeration or sintering [26,27].

2. Results and Discussions

2.1. Crystalline Structures

Figure 1 shows powder X-ray diffraction (XRD) patterns of three series of catalysts: Au/silica, Pt/silica and Au-Pt/silica, and the XRD patterns of the pure silica supports confirmed their amorphous structures (as given in Figure S1a, ESI). In Figure 1a, two distinguished diffraction peaks at 2θ of 38.2° and 44.3° were observed on the series of Au/silica, which were assigned to (111) and (200) reflections of metallic Au, respectively [11,13]. For the series of Pt/silica as shown in Figure 1b, two significant diffraction peaks at 2θ of 39.7° and 46.3° were observed, corresponding to (111) and (200) facets of metallic Pt, respectively [28,29]. As expected, four diffraction peaks at 38.2°, 44.3°, 39.7° and 46.3° were observed on the bimetallic Au-Pt/silica catalysts as shown in Figure 1c, demonstrating the formation of Au-Pt bimetallic particles on the catalysts of Au-Pt/silica. None of the aforementioned four diffraction peaks were observed on pure silica supports (Figure S1a), and the obvious diffraction peaks of both monometallic and bimetallic catalysts revealed that monometallic Au, Pt and bimetallic Au-Pt metal particles were well formed and dispersed on the silica supports. Moreover, the peak positions of Au NPs or Pt NPs in Au-Pt/silica did not shift, compared with those in Au/silica or Pt/silica, respectively, which suggested that Au NPs and Pt NPs were separate from each other and did not form alloy structures under synthetic conditions.

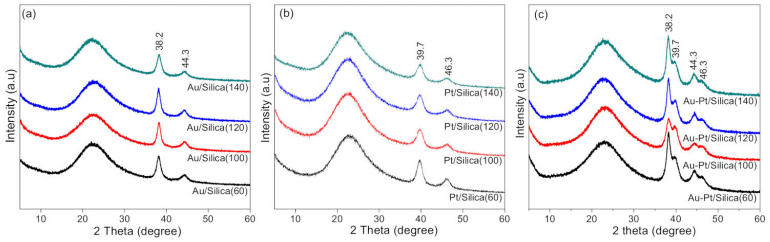

Figure 1. Powder XRD patterns of as-made three series of catalysts of (**a**) Au/silica, (**b**) Pt/silica, and (**c**) Au-Pt/silica.

2.2. Optical Properties

In Figure 2a, the UV-Vis spectra of Au/silica catalysts were displayed (only the visible light region), and the peaks which were the localized surface plasmon resonance (LSPR) bands could be observed clearly. The LSPR effect was generated by the collective oscillation of electrons of Au NPs along with the electromagnetic field of visible light, and it has been well studied in our previous work on zeolites supported Au NPs [5,30]. The LSPR band of these four Au/silica catalysts all centered around 522 nm, demonstrating that the particle sizes of Au NPs were similar (this result will be confirmed by Transmission Electron Microscopy (TEM) analyses). Pt NPs showed no LSPR effect in the visible light region (Figure 2b), just like the spectra of silica supports (as given in Figure S1b). Figure 2c showed that the presence of Pt NPs did not suppress or enhance the LSPR bands of Au NPs, suggesting that Au NPs were not affected by Pt NPs significantly. Nevertheless, the LSPR band shifted very slightly to longer wavelength, which was possibly due to the fact that a small proportion of the free electrons of Pt NPs contributed to Au NPs (this phenomenon will be confirmed later by X-ray Photoelectron Spectroscopy (XPS) analyses on the oxidation state of Au and Pt over silica supports). These UV-Vis results were unable to directly demonstrate the structure of the bimetallic active sites, but they implied the formation of both Au NPs and Pt NPs separately (not alloy), and these were consistent with the observation of XRD analyses.

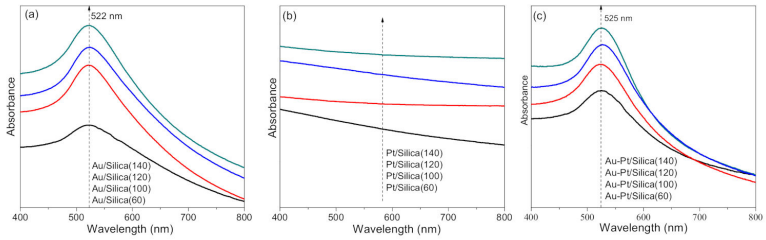

Figure 2. UV-Vis spectra of three series of catalysts of (**a**) Au/silica, (**b**) Pt/silica, and (**c**) Au-Pt/silica.

2.3. Textural Properties

N_2 adsorption-desorption isotherms and pore size distributions of three series of catalysts (Au/silica, Pt/silica, and Au-Pt/silica) are shown in Figure 3, and the textural properties are summarized in Table 1. For pure silica supports, the N_2 adsorption-desorption isotherms and the Barrett-Joyner-Halenda (BJH) analyses are provided in Figure S2 and Table S1. Figure S2a displayed the isotherms of four silica supports and showed clearly that the porosity was successfully controlled by varying the synthetic temperatures. The silica prepared at 60 °C, denoted as silica(60), had no pores. The silica(100) showed the Type I adsorption-desorption isotherm, as the in-pore monolayer-adsorption amount N_2 was saturated in a low relative pressure region of $P/P_0 < 0.05$. The silica(120) showed both the Type I adsorption ($P/P_0 < 0.05$) and the Type IV adsorption curves with capillary condensation at the region of P/P_0 of 0.4–0.7 and a similarity to the H2 hysteresis loop in the desorption isotherm. The silica(140) showed both the Type I adsorption ($P/P_0 < 0.05$) and the Type IV adsorption curves at the region of P/P_0 of 0.4–0.8 and a similarity to the H1 hysteresis loop, demonstrating clearly the co-existence of

hierarchical micropores and mesopores. The mesopore diameters increased from 3.0 nm to 4.1 nm (Table S1) as the synthetic temperatures raised from 100 °C to 140 °C and the pore diameter distribution was given in Figure S2b. Moreover, the surface area varied as increasing the synthetic temperatures, but the silica(140) which had the most mesopores showed a declined surface area (536.8 m^2/g) (Table S1).

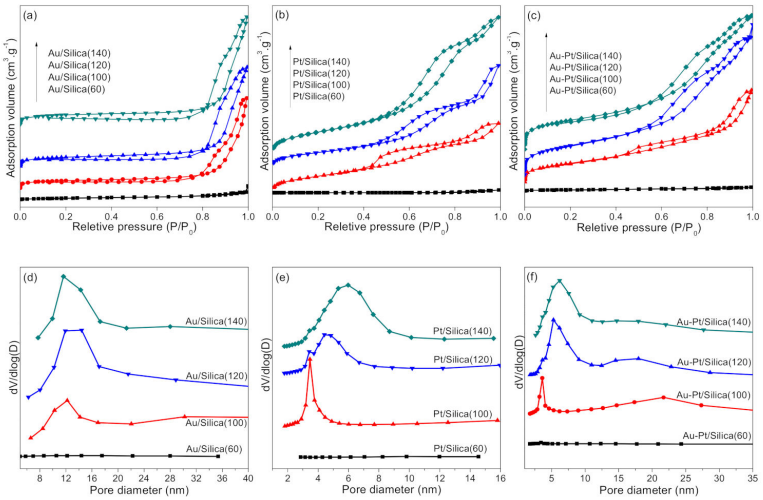

Figure 3. N_2 adsorption-desorption isotherms of (**a**) Au/silica, (**b**) Pt/silica, and (**c**) Au-Pt/silica; BJH pore size distribution of (**d**) Au/silica, (**e**) Pt/silica, and (**f**) Au-Pt/silica.

Table 1. Surface areas, pore volumes and pore diameters of Au/Silica, Pt/Silica and Au-Pt/Silica.

Samples	S_{BET} [a] (m^2 g^{-1})	V_t [b] (cm^3 g^{-1})	D_p [c] (nm)
Au/Silica(140)	144.4	0.702	16.2
Au/Silica(120)	135.8	0.647	15.8
Au/Silica(100)	110.8	0.587	18.4
Au/Silica(60)	24.3	0.085	–
Pt/Silica(140)	290.5	0.537	5.6
Pt/Silica(120)	192.2	0.325	5.1
Pt/Silica(100)	211.7	0.278	4.2
Pt/Silica(60)	2.5	0.007	–
Au-Pt/Silica(140)	328.3	0.656	7.0
Au-Pt/Silica(120)	334.2	0.738	7.0
Au-Pt/Silica(100)	216.9	0.453	6.6
Au-Pt/Silica(60)	14.7	0.017	–

[a] BET surface area. [b] BJH desorption pore volume. [c] BJH desorption mean pore size.

As described in the following section, Au NPs and/or Pt NPs were introduced by the sol-immobilization method using the pre-prepared Au colloids and/or Pt colloids under ultrasonic conditions. For the silica(60), the loading efficiency was very low, because the target metal loading was 3% wt, whereas the actual loading was only lower than 0.5% wt, and no pores were created after loading of metal NPs. On the contrary, the surface areas decreased considerably owing to the loading of metal NPs (Table 1). Interestingly, for silica(100), silica(120) and silica(140) which had hierarchical micro-mesoporous structures, after introduction of metal NPs, more mesopores and macropores were created (revealed by hysteresis loops), whereas the micropores remarkably decreased. The change in porosity of silica supports was due to the fact that the alkaline solution of metal colloids slowly destructed the micropores and mesorpores by desilication (this desilication strategy is a well-known approach to prepare hierarchical porous zeolites) [23–25]. In general, the surface area of catalysts decreased to different degrees, compared with their counterparts of pure silica supports.

In detail, for the series of Au/silica catalysts, the surface areas increased from 24.3 m^2/g to 144.4 m^2/g as the function of synthetic temperatures from 60 °C to 140 °C, and the pore volume increased from 0.085 cm^3/g to 0.702 cm^3/g (Table 1). The mesopore diameters centered at around 12 nm except Au/silica(60) as shown in Figure 3d, whereas the determined average pore diameter was around 17 ± 2 nm owing to the existence of macropores (Figure 3a). For the series of Pt/silica catalysts, the surface areas varied from 2.5 m^2/g to 290 m^2/g for all catalysts, and the pore diameters increased from 4.2 nm and 5.6 nm (Table 1 and Figure 3e) for the catalysts of Pt/silica(100), Pt/silica(120) and Pt/silica(140). For the series of Au-Pt/silica catalysts, the surface areas increased from 14.7 m^2/g to 328.3 m^2/g for the four catalysts, and the pore diameters increased from 6.6 nm and 7.0 nm (Table 1 and Figure 3e) for the catalysts of Au-Pt/silica(100), Au-Pt/silica(120) and Au-Pt/silica(140). These results demonstrated that the catalysts with controlled hierarchical pore structures were successfully prepared.

2.4. Morphologies of Catalysts and Particle Size of Metal NPs

TEM images of catalysts were collected to investigate the morphologies of catalysts and particle sizes of metal NPs as shown in Figure 4. No ordered channel structures of silica supports were observed by TEM images [13], and the histograms of particle size distribution of Au/silica, Pt/silica and Au-Pt/silica showed that Au NPs and/or Pt NPs were uniformly distributed on the silica supports. In general, the average size of Au NPs on Au/silica (10 ± 2 nm) was larger than that of Pt NPs on Pt/silica (6 ± 2 nm), and the average particle size of metal NPs on Au-Pt/silica was 7 ± 2 nm. For each series of catalysts with monometallic loading, the metal particle size was relatively uniform, and this result demonstrated that the sol-immobilization method was effective in preparing supported Au or Pt NPs with controlled sizes on porous silica supports.

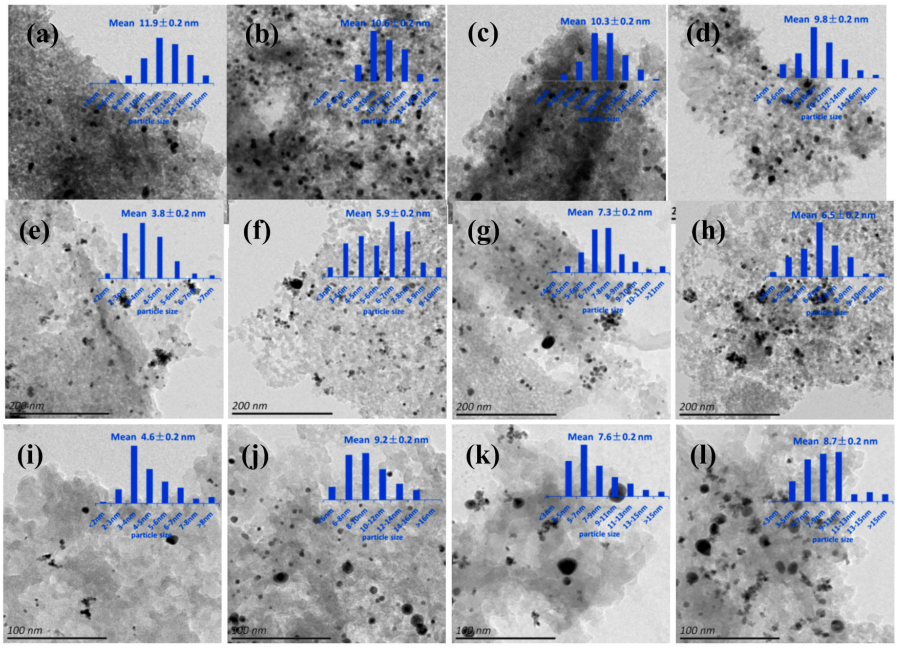

Figure 4. TEM images of (**a**) Au/silica(60), (**b**) Au/silica(100), (**c**) Au/silica(120) and (**d**) Au/silica(140); (**e**) Pt/silica(60), (**f**) Pt/silica(100), (**g**) Pt/silica(120) and (**h**) Pt/silica(140); (**i**) Au-Pt/silica(60), (**j**) Au-Pt/silica(100), (**k**) Au-Pt/silica(120) and (**l**) Au-Pt/silica(140). Insets are histograms of metal particle size distribution.

2.5. Elemental and XPS Analyses

The actual metal loading of each catalyst determined by ICP-MS was provide in Table S2; generally the loading efficiency on silica(60) was extremely low owing to poor surface areas (Table 1). For Au/silica catalysts, the target gold loading was 3% wt, and the results showed that the loading efficiency was

high over silica(100), silica(120) and silica(140) which had hierarchical porous structures, whereas it was relatively lower for Pt/silica catalysts. For the Au-Pt/silica catalysts, the target metal loading was 1.5% wt for Au or Pt, and the results demonstrated that this sol-immobilization method worked well in preparing bimetallic Au-Pt/silica catalysts when the pore structures were well controlled. Overall, the high efficiency of metal loading was ascribed to the stabilization effect of channels in the porous silica and these phenomena have been generally recognized, using other ordered mesoporous materials such as SBA-15 and MCM-41 [31,32].

The electronic properties of the surface elements of a series of Au/silica, Pt/silica and Au-Pt/silica catalysts were characterized by XPS. The XPS spectra of Au 4f and Pt 4f are shown in Figure 5, and the proportions of a metal with different oxidation sates are given in Table S2. For Au/silica catalysts as shown in Figure 5a, they exhibited two strong peaks at 83.6 eV (Au $4f_{7/2}$) and 87.3 eV (Au $4f_{5/2}$) [33,34], indicating the presence of metallic gold species. Except Au/silica(60), the other three Au/silica catalysts also showed two peaks which shifted to higher binding energy at 85.2 eV ($4f_{7/2}$) and 88.9 eV (Au $4f_{5/2}$), assigning to positively charged gold species ($Au^{\delta+}$) according to literature reports [15,29]. These results indicated that Au NPs loaded on porous silica were affected electronically by supports in a more significant way, compared with those loaded on silica(60). For Pt/silica catalysts as illustrated in Figure 5b, the two strong peaks at 71.5 eV (Pt $4f_{7/2}$) and 74.8 eV (Pt $4f_{5/2}$) [28,29] indicated the presence of metallic Pt species. In addition, the detailed oxidation state analyses showed that two peaks with binding energy at 72.8 eV (Pt $4f_{7/2}$) and 76.1 eV (Pt $4f_{5/2}$) were observed, and they were assigned to positively charged platinum species ($Pt^{\delta+}$) [35]. These results suggested that the electronic properties of Pt NPs were also influenced by silica supports (Table S2), and this phenomena were also observed in our previous study [31]. Interestingly, when Au NPs and Pt NPs were loaded together onto silica, the oxidation sate of gold was dominantly metallic gold species, whereas Pt NPs still showed positively charged species (Figure 5c and Table S2), probably because Au NPs which had stronger electronegativity attracted free electrons on Pt NPs as reported in some studies [29,36]. The XPS analyses on Au-Pt/silica further confirmed the co-existence Au and Pt over silica supports as demonstrated by the powder XRD patterns and provided more information on their electron interaction.

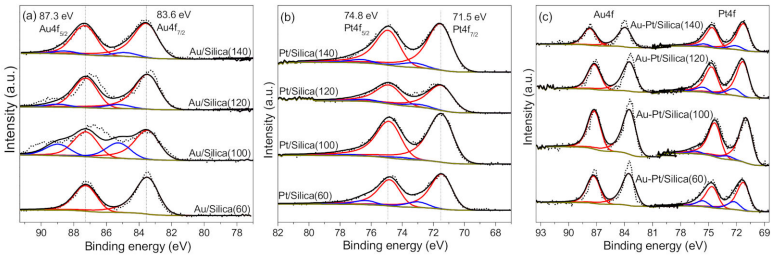

Figure 5. XPS spectra of (**a**) Au 4f of a series of Au/silica; (**b**) Pt 4f of a series of Pt/silica; (**c**) Au 4f and Pt 4f of a series of Au-Pt/silica.

2.6. Catalytic Performance and Discussions on the Steric Effects

The above characterizations demonstrated that Au NPs, Pt NPs, or Au-Pt NPs were successfully loaded on silica supports with hierarchical porous structures, whereas silica(60) had a poor loading efficiency of these metal NPs. Now one may wonder how and why the hierarchical porous structures of catalysts affect their catalytic performance in reactions. To verify the hypothesis, the selective oxidation of aromatic alcohols was selected as model reactions to evaluate the steric effect of hierarchical porous structures on the catalytic conversions and reaction rates.

Figure 6a showed the conversions of benzyl alcohol over these twelve catalysts, and Au/silica(60) exhibited poor performance owing to the very low loading of metal NPs. For the other three catalysts of Au/silica(100), Au/silica(120) and Au/silica(140), they exhibited the highest catalytic conversions compared with other series of catalysts, and these three catalysts showed similar catalytic conversions and excellent selectivity toward benzaldehyde (>99%, not shown in the figures), and no other products

were detectable under experimental conditions. On the contrary, the conversions of benzyl alcohol over Pt/silica(100), Pt/silica(120) and Pt/silica(140) were quite low, owing to the poor activity of Pt NPs to catalyze the selective oxidation reactions under experimental conditions. The conversions of benzyl alcohol over Au-Pt/silica(100), Au-Pt/silica(120) and Au-Pt/silica(140) were lower than those on the corresponding Au/silica(100), Au/silica(120), and Au/silica(140), respectively, owing to the lower content of gold loading and poor catalytic activity of Pt NPs. Interestingly, the conversions of benzyl alcohol over Au-Pt/silica(100), Au-Pt/silica(120) and Au-Pt/silica(140) increased significantly as the porosity of silica supports increased. These phenomena encouraged us to investigate into the underlying mechanism on the differences in catalytic conversions over the Au-Pt/silica catalysts.

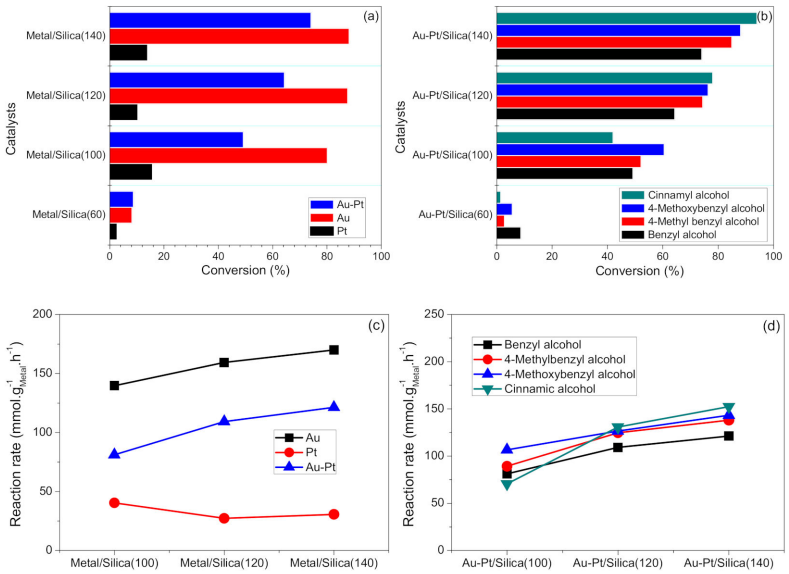

Figure 6. (**a**) Conversions of benzyl alcohol over Au/silica, Pt/silica, and Au-Pt/silica. (**b**) Conversions of different aromatic alcohols over Au/silica, Pt/silica, and Au-Pt/silica. (**c**) Reaction rates of benzyl alcohol over Au/silica, Pt/silica, and Au-Pt/silica. (**d**) Reaction rates of different aromatic alcohols over Au/silica, Pt/silica, and Au-Pt/silica. **Note**: the reaction rate was calculated on the basis of the mass of Au, Pt, or Au-Pt. **Reaction conditions**: 3.5 mmol reactant, 20 mL toluene, 0.35 mmol NaOH, 0.2 g catalyst, 90 °C, 4 h).

In the preparation of Au-Pt/silica catalyst except Au-Pt/silica(60), the particle sizes of Au NPs and Pt NPs were pre-controlled by colloid synthesis. They exhibited similar crystal structures (Figure 1c), optical properties (Figure 2c), and average particle sizes (Figure 4j–l) of metal NPs, the loading contents of metals were similar, as detected by ICP-MS (Table S2), and the oxidation sates were also similar, as determined by XPS analyses (Figure 5c and Table S2). Hence, the change in catalytic conversions and reaction rates (as given in Figure 6c) should be primarily resulted from the various hierarchical porous structures as confirmed by BET and BJH analyses (Figure 3c,f). On the basis of these analyses, it could be deduced that the hierarchical porous structures had a steric effect on the diffusion of reactants, and this steric effect was a dominating reason for the change in catalytic performance over Au-Pt/silica(100), Au-Pt/silica(120) and Au-Pt/silica(140). To further confirm these observations, other typical aromatic alcohols, such as 4-methyl benzyl alcohol, 4-methoxy benzyl alcohol, and cinnamic alcohol, were also tested over these Au-Pt/silica catalysts. As shown in Figure 6b,d, the conversions and reaction rates of each alcohol also increased markedly over Au-Pt/silica(100), Au-Pt/silica(120) and Au-Pt/silica(140). These results confirmed that the steric effect of hierarchical porous structures controlled the diffusion of reactant molecules and thus the reaction rates of them over Au-Pt/silica catalysts.

3. Experimental Section

3.1. Raw Materials

Polyethylene-polypropylene glycol (P123, ~Mn 5800) was purchased from Macklin (Shanghai, China). Tetraethyl orthosilicate (TEOS, SiO_2 ≥ 28.4 wt%), hydrochloric acid (HCl, 36–38 wt%) and potassium hydroxide (≥85%, KOH) were purchased from Sinopharm Chemical Reagent Company Co. Ltd., China. Sodium boronhydride (≥90%, $NaBH_4$) was purchased from Nanjing Chemical Reagent Co. Ltd., China. Poly (diallyldimethylammonium chloride) solution (PDDA, 20 wt.% in water) and chloroplatinic acid hexahydrate ($H_2PtCl_6{\cdot}6H_2O$) were purchased from Aladdin Industrial Inc. (Shanghai, China). Chloroauric acid ($HAuCl_4$) was purchased from Macklin (Shanghai, China).

Benzyl alcohol (≥99%) was purchased from Shanghai Lingfeng Chemical Reagent Co. Ltd., China. Cinnamic alcohol (≥98%) was purchased from Shanghai Xushuo Biotechnology Co. Ltd., China. Toluene (≥99.5%) was purchased from Nanjing Chemical Reagent Co. Ltd., China. 4-Methylbenzyl alcohol (98%) and 4-methoxybenzyl alcohol (98%) were purchased from Aladdin Industrial Inc. (Shanghai, China). Sodium hydroxide (≥96%, NaOH) was purchased from Sinopharm Chemical Reagent Company Co. Ltd., China. The oxygen was from the BOC (99.99%). All products were used as received without further purification.

3.2. Catalyst Preparation

Synthesis of silica. The silica supports were prepared by a modified method as reported in the literature [37]. Pluronic P123 (2 g) was dissolved in hydrochloric acid (2 M HCl, 70 cm^3) under stirring at 35 °C for 4 h. TEOS (4.7 cm^3) was added dropwise and the solution continuously agitated for 24 h. The resulting gel was aged for 24 h at 60 °C, 100 °C, 120 °C and 140 °C without agitation and the solid product filtered, washed with water thoroughly until the pH was <9. After drying at 80 °C overnight the final material was subsequently following 550 °C calcination in air for 5 h (ramp 1 °C · min^{-1}) to remove the organic species. These supports were denoted as silica(60) (silica without pores as a reference), silica(100), silica(120) and silica(140), corresponding to the aging temperature at 60 °C, 100 °C, 120 °C, and 140 °C, respectively.

Preparation of Au colloids and Pt colloids: These two types of metal colloids were prepared according to the method as reported in the literature [38]. 5.2 mL of $HAuCl_4$ (chloroauric acid) aqueous solution (5.8 $g_{Au}{\cdot}L^{-1}$) was prepared. 3 mL of 0.1 M KOH aqueous solution was added under vigorous stirring and subsequently, the appropriate polymer solution (0.3 g of PDDA in 15 mL water). A freshly prepared aqueous solution of the reducing agent (aqueous solution of 0.35 M $NaBH_4$, 15 mL) was added, resulting quickly in a red sol within a few seconds. Afterwards, the mixture was stirred for an hour at room temperature and aged for 24 h. The Pt colloids were prepared following an identical procedure, and the metal source was 7.96 mL aqueous $H_2PtCl_6{\cdot}6H_2O$ (chloroplatinic acid hexahydrate) solution.

Catalysts preparation: Loading of metal NPs onto silica was conducted following the procedure: Powders of silica supports (1 g) were dispersed in the suspension of Au or Pt colloids with aforementioned to achieve a nominal mass loading of 3 wt%. The mixture was subject to vigorous stirring for 1 h and then sonication for 1 h, and this stirring-sonication process was repeated three times to ensure a uniform contact between metal colloids and silica supports. After this, the mixture was aged for 24 h and then the solid was separated, thoroughly washed with water and ethanol to remove soluble residues, and dried at 80 °C overnight. Catalysts of Au-Pt/silica were prepared following an identical procedure, with a target Au or Pt loading of 1.5 wt%, namely half of the as-prepared Au colloids and half of the Pt colloids were mixed and stirred for 1 h to reach a total nominal mass loading of 3 wt%. The resulting solid was collected, dried, and used directly as catalysts.

3.3. Catalyst Characterization

N_2 porosimetry was performed on samples degassed at 120 °C for 4 h before analysis using a Micromeritics ASAP 2020 at −196 °C porosimeter, with BET surface areas being calculated over the range P/P_0 = 0.03–0.19, wherein a linear relationship was maintained. Pore size distributions were obtained applying the BJH model to the desorption branch of the isotherm for relative pressures between 0.35–0.975. Structural order was evaluated by means of powder X-ray Diffraction (XRD) on a Bruker D8 Advance diffractometer using the Cu K_α line in the range 2θ = 5–60° with a step size of 5°. The morphologies of the samples were observed by Scanning Electron Microscopy (SEM) using a JSM-7600F (JEOL Ltd., Japan) with an operating voltage of 30 kV. The bulk Au and Pt actual loadings were determined by the Inductive Coupled Plasma mass spectrometry (ICP-MS, NeXion 300X PE Ltd., USA) instrument, and the sample was dissolved in aqua regia solution under ultrasonic condition for 4 h until complete dissolution. Transmission Electron Microscopy (TEM) image and high-resolution transmission electron microscope (HRTEM) were obtained by a JEOL JEM-2100 instrument at the accelerating voltage of 200 kV. X-ray Photoelectron Spectroscopy (XPS) measurements were conducted using a photoelectron spectrometer (AXIS UltraDLD, Japan) equipped with a charge neutralizer and the Al K_α X-ray source ($h\nu$ = 1486.6 eV). All the binding energies were referenced to the C1s peak at 284.6 eV of the surface adventitious carbon. Shirley background-subtracted Au and Pt 4f XP spectra were fitted using CasaXPS version 2.3.14 adopting a common asymmetric peak shape. UV-vis diffuse reflectance spectra (DRS) was determined with an UV-2600 (Shimadzu, Japan) spectrophotometer.

3.4. Catalytic Tests

The reaction was conducted in a 50 mL round-bottomed Pyrex glass flask as a reactor with a sealed spigot and a magnetic stirrer. Catalytic oxidation of aromatic alcohol was conducted under the oxygen atmosphere. Typically, 3.5 mmol of aromatic alcohol, 20 mL of toluene as solvent, and 0.35 mmol of NaOH were mixed in the reactor, followed by adding 200 mg of the catalyst (Note: a small proportion of NaOH could activate the reactants of alcohols and the molecular ration between NaOH and reactant was no larger than 1:10 [10]). Under dark conditions, the mixed suspension was stirred for 2 h at room temperature to reach the adsorption equilibrium. Then flask was purged with oxygen for more than 1 min to remove air and then sealed. The reactor was stirred during reaction in an oil bath for 4 h at 90 °C. During these reactions, 1 mL aliquots were collected using syringes and filtered through a millipore filter (pore size 0.22 μm) to remove the catalyst particulates. The filtrates were analyzed by an FULI 9790II Gas Chromatograph (GC) with the PEG-20M column (column temperature: 150 °C, injector temperature: 200 °C, FID temperature: 250 °C). Quantities of the products and reactants were calculated from the peak areas of the standard compounds using calibration curves, and these standard compounds were commercial ones.

4. Conclusions

The selective oxidation of aromatic alcohols to their corresponding aldehydes over Au-Pt/silica catalysts with different pore diameters were investigated. The characterization results of XRD, UV-Vis and TEM confirmed the formation and well-distribution of Au NPs and/or Pt NPs on the hierarchical porous silica supports, and the BET and BJH analyses revealed the porosity of the parent silica supports and the evolution of pore structures after loading of Au NPs and/or Pt NPs. The experimental results showed that the catalytic performance in terms of conversions and reaction rates were correlated with the hierarchical porous structures of catalysts, and the steric effect of Au-Pt/silica catalysts were well-demonstrated. This study offers inspiring observations for catalyst design using metal nanoparticles and porous supports, as the diffusion effect of reactants, intermediates or products is considerable particularly in organic conversions [39,40].

Supplementary Materials: The following are available online at http://www.mdpi.com/2073-4344/10/10/1192/s1, Figure S1: (a) Powder XRD patterns and (b) UV-Vis spectra (the visible light region) of silica supports, Table S1: Physical properties of SBA-15.

Author Contributions: J.Y. carried out experiments and analyzed the data. L.S. helped data curation and analyzed the data. X.G. supervised the research project and revised the manuscript. X.Z. designed the study and wrote the original manuscript. J.C. revised the manuscript and checked the English language. All authors have read and agreed to the published version of the manuscript.

Funding: This research was supported by the National Natural Science Foundation of China (NNSFC21706134) and the Young Natural Science Foundation of Jiangsu Province (BK20170918).

Acknowledgments: Thank the technical support from the "Advanced Analysis and Testing Centre of Nanjing Forestry University".

Conflicts of Interest: The authors declare no conflict of interest.

References

1. Chen, B.; Wang, L.Y.; Gao, S. Recent advances in aerobic oxidation of alcohols and amines to imines. *ACS Catal.* **2015**, *5*, 5851–5876. [CrossRef]
2. Zhang, X.G.; Wilson, K.; Lee, A.F. Heterogeneously catalyzed hydrothermal processing of C_5-C_6 sugars. *Chem. Rev.* **2016**, *116*, 12328–12368. [CrossRef] [PubMed]
3. Guo, Z.; Liu, B.; Zhang, Q.H.; Deng, W.P.; Wang, Y.; Yang, Y.H. Recent advances in heterogeneous selective oxidation catalysis for sustainable chemistry. *Chem. Soc. Rev.* **2014**, *43*, 3480–3524. [CrossRef] [PubMed]
4. Mallat, T.; Baiker, A. Oxidation of alcohols with molecular oxygen on solid catalysts. *Chem. Rev.* **2004**, *104*, 3037–3058. [CrossRef] [PubMed]
5. Zhang, X.G.; Ke, X.B.; Zhu, H.Y. Zeolite-supported gold nanoparticles for selective photooxidation of aromatic alcohols under visible-light irradiation. *Chem. Eur. J.* **2012**, *18*, 8048–8056. [CrossRef]
6. Yadav, G.D.; Mehta, P.H. Theoretical and experimental analysis of capsule membrane phase transfer catalysis: Selective alkaline hydrolysis ofbenzyl chloride to benzyl alcohol. *Catal. Lett.* **1993**, *21*, 391–403. [CrossRef]
7. Konietzni, F.; Zanthoff, H.W.; Maier, W.F. The role of active oxygen in the AMM-VxSi-catalysed selective oxidation of toluene. *J. Catal.* **1999**, *188*, 154–164. [CrossRef]
8. Martin, A.; Bentrup, U.; Wolf, G.U. The effect of alkali metal promotion on vanadium-containing catalysts in the vapour phase oxidation of methyl aromatics to the corresponding aldehydes. *Appl. Catal. A Gen.* **2002**, *227*, 131–142. [CrossRef]
9. Aellig, C.; Girard, C.; Hermans, I. Aerobic alcohol oxidations mediated by nitric acid. *Angew. Chem. Int. Ed.* **2011**, *50*, 12355–12360. [CrossRef]
10. Yuan, Z.F.; Zhao, W.N.; Liu, Z.P.; Xu, B.Q. NaOH alone can be a homogeneous catalyst for selective aerobic oxidation of alcohols in water. *J. Catal.* **2017**, *353*, 37–43. [CrossRef]
11. Lavenn, C.; Demessence, A.; Tuel, A. $Au_{25}(SPh\text{-}pNH_2)_{17}$ nanoclusters deposited on SBA-15 as catalysts for aerobic benzyl alcohol oxidation. *J. Catal.* **2015**, *322*, 130–138. [CrossRef]
12. Liu, C.H.; Lin, C.Y.; Chen, J.L.; Lu, K.T.; Lee, J.F.; Chen, J.M. SBA-15-supported Pd catalysts: The effect of pretreatment conditions on particle size and its application to benzyl alcohol oxidation. *J. Catal.* **2017**, *350*, 21–29. [CrossRef]
13. Wu, P.P.; Cao, Y.X.; Zhao, L.M.; Wang, Y.; He, Z.K.; Xing, W.; Bai, P.; Mintova, S.; Yan, Z.F. Formation of PdO on Au-Pd bimetallic catalysts and the effect on benzyl alcohol oxidation. *J. Catal.* **2019**, *375*, 32–43. [CrossRef]
14. Tang, Q.H.; Gong, X.N.; Zhao, P.Z.; Chen, Y.T.; Yang, Y.H. Copper-manganese oxide catalysts supported on alumina: Physicochemical features and catalytic performances in the aerobic oxidation of benzyl alcohol. *Appl. Catal. A Gen.* **2010**, *389*, 101–107. [CrossRef]
15. Wang, T.; Yuan, X.; Li, S.R.; Zeng, L.; Gong, J.L. CeO_2-modified Au@SBA-15 nanocatalysts for liquid-phase selective oxidation of benzyl alcohol. *Nanoscale* **2015**, *7*, 7593–7602. [CrossRef]
16. Tang, H.L.; Wei, J.K.; Liu, F.; Qiao, B.T.; Pan, X.L.; Li, L.; Liu, J.Y.; Wang, J.H.; Zhang, T. Strong metal-support interactions between gold nanoparticles and nonoxides. *J. Am. Chem. Soc.* **2016**, *138*, 56–59. [CrossRef]
17. Liu, Y.L.; Chen, H.; Xu, C.J.; Sun, Y.M.; Li, S.; Qin, G.W. Control of catalytic activity of nano-au through tailoring the fermi level of support. *Small* **2019**, *15*. [CrossRef] [PubMed]

18. Chen, Y.T.; Lim, H.M.; Tang, Q.H.; Gao, Y.T.; Sun, T.; Yan, Q.Y.; Yang, Y.H. Solvent-free aerobic oxidation of benzyl alcohol over Pd monometallic and Au-Pd bimetallic catalysts supported on SBA-16 mesoporous molecular sieves. *Appl. Catal. A Gen.* **2010**, *380*, 55–65. [CrossRef]
19. Olmos, C.M.; Chinchilla, L.E.; Villa, A.; Delgado, J.J.; Hungria, A.B.; Blanco, G.; Prati, L.; Calvino, J.J.; Chen, X.W. Size, nanostructure, and composition dependence of bimetallic Au-Pd supported on ceria-zirconia mixed oxide catalysts for selective oxidation of benzyl alcohol. *J. Catal.* **2019**, *375*, 44–55. [CrossRef]
20. Ishida, T.; Murayama, T.; Taketoshi, A.; Haruta, M. Importance of size and contact structure of gold nanoparticles for the genesis of unique catalytic processes. *Chem. Rev.* **2020**, *120*, 464–525. [CrossRef]
21. Sankar, M.; He, Q.; Engel, R.V.; Sainna, M.A.; Logsdail, A.J.; Roldan, A.; Willock, D.J.; Agarwal, N.; Kiely, C.J.; Hutchings, G.J. Role of the support in gold-containing nanoparticles as heterogeneous catalysts. *Chem. Rev.* **2020**, *120*, 3890–3938. [CrossRef] [PubMed]
22. van Deelen, T.W.; Mejia, C.H.; de Jong, K.P. Control of metal-support interactions in heterogeneous catalysts to enhance activity and selectivity. *Nat. Catal.* **2019**, *2*, 955–970. [CrossRef]
23. Yang, S.T.; Yu, C.X.; Yu, L.L.; Miao, S.; Zou, M.M.; Jin, C.Z.; Zhang, D.Z.; Xu, L.Y.; Huang, S. Bridging dealumination and desilication for the synthesis of hierarchical MFI zeolites. *Angew. Chem. Int. Ed.* **2017**, *56*, 12553–12556. [CrossRef] [PubMed]
24. Wilde, N.; Pelz, M.; Gebhardt, S.G.; Glaser, R. Highly efficient nano-sized TS-1 with micro-/mesoporosity from desilication and recrystallization for the epoxidation of biodiesel with H_2O_2. *Green Chem.* **2015**, *17*, 3378–3389. [CrossRef]
25. Wang, D.R.; Xu, L.; Wu, P. Hierarchical, core-shell meso-ZSM-5@mesoporous aluminosilicate-supported Pt nanoparticles for bifunctional hydrocracking. *J. Mater. Chem. A* **2014**, *2*, 15535–15545. [CrossRef]
26. Wang, N.; Sun, Q.M.; Yu, J.H. Ultrasmall metal nanoparticles confined within crystalline nanoporous materials: A fascinating class of nanocatalysts. *Adv. Mater.* **2019**, *31*. [CrossRef]
27. Ma, C.Y.; Dou, B.J.; Li, J.J.; Cheng, J.; Hu, Q.; Hao, Z.P.; Qiao, S.Z. Catalytic oxidation of benzyl alcohol on Au or Au-Pd nanoparticles confined in mesoporous silica. *Appl. Catal. B Environ.* **2009**, *92*, 202–208. [CrossRef]
28. Li, B.; Xu, Z.X.; Jing, F.L.; Luo, S.Z.; Chu, W. Facile one-pot synthesized ordered mesoporous Mg-SBA-15 supported PtSn catalysts for propane dehydrogenation. *Appl. Catal. A Gen.* **2017**, *533*, 17–27. [CrossRef]
29. Wu, P.P.; Cao, Y.X.; Wang, Y.; Xing, W.; Zhong, Z.Y.; Bai, P.; Yan, Z.F. Ultrastable bimetallic catalyst with tuned surface electronic properties for highly selective oxidation of cyclohexane. *Appl. Surf. Sci.* **2018**, *457*, 580–590. [CrossRef]
30. Zhang, X.G.; Du, A.J.; Zhu, H.Y.; Jia, J.F.; Wang, J.; Ke, X.B. Surface plasmon-enhanced zeolite catalysis under light irradiation and its correlation with molecular polarity of reactants. *Chem. Commun.* **2014**, *50*, 13893–13895. [CrossRef]
31. Zhang, X.G.; Durndell, L.J.; Isaacs, M.A.; Parlett, C.M.A.; Lee, A.F.; Wilson, K. Platinum-catalyzed aqueous-phase hydrogenation of D-glucose to D-sorbitol. *ACS Catal.* **2016**, *6*, 7409–7417. [CrossRef]
32. Hamza, A.; Srinivas, D. Selective oxidation of benzyl alcohol over copper phthalocyanine immobilized on MCM-41. *Catal. Lett.* **2009**, *128*, 434–442. [CrossRef]
33. Chen, Y.; Li, W.Z.; Wang, J.Y.; Yang, Q.; Hou, Q.D.; Ju, M.T. Gold nanoparticle-modified TiO_2/SBA-15 nanocomposites as active plasmonic photocatalysts for the selective oxidation of aromatic alcohols. *RSC Adv.* **2016**, *6*, 70352–70363. [CrossRef]
34. Escamilla-Perea, L.; Peza-Ledesma, C.L.; Nava, R.; Rivera-Munoz, E.M.; Pawelec, B.; Fierro, J.L.G. CO oxidation at 20 degrees C over Au/SBA-15 catalysts decorated by Fe_2O_3 nanoparticles. *Catal. Commun.* **2011**, *15*, 108–112. [CrossRef]
35. Wang, G.M.; Yao, R.H.; Xin, H.Y.; Guan, Y.J.; Wu, P.; Li, X.H. At room temperature in water: Efficient hydrogenation of furfural to furfuryl alcohol with a Pt/SiC-C catalyst. *RSC Adv.* **2018**, *8*, 37243–37253. [CrossRef]
36. Tang, H.L.; Su, Y.; Zhang, B.S.; Lee, A.F.; Isaacs, M.A.; Wilson, K.; Li, L.; Ren, Y.G.; Huang, J.H.; Haruta, M.; et al. Classical strong metal-support interactions between gold nanoparticles and titanium dioxide. *Sci. Adv.* **2017**, *3*. [CrossRef]
37. Zhao, D.; Feng, J.; Huo, Q.; Melosh, N.; Fredrickson, G.H.; Chmelka, B.F.; Stucky, G.D. Triblock copolymer syntheses of mesoporous silica with periodic 50 to 300 angstrom pores. *Science* **1998**, *279*, 548–552. [CrossRef]
38. Mirescu, A.; Prusse, U. Selective glucose oxidation on gold colloids. *Catal. Commun.* **2006**, *7*, 11–17. [CrossRef]

39. Xu, L.; Peng, H.G.; Zhang, K.; Wu, H.H.; Chen, L.; Liu, Y.M.; Wu, P. Core-shell-structured titanosilicate as a robust catalyst for cyclohexanone ammoximation. *ACS Catal.* **2013**, *3*, 103–110. [CrossRef]
40. Dapsens, P.Y.; Mondelli, C.; Perez-Ramirez, J. Highly selective Lewis acid sites in desilicated MFI zeolites for dihydroxyacetone isomerization to lactic acid. *ChemSusChem* **2013**, *6*, 831–839. [CrossRef] [PubMed]